TTSA3R: Training-Free Temporal-Spatial Adaptive Persistent State for Streaming 3D Reconstruction

Zhijie Zheng, Xinhao Xiang, Jiawei Zhang

University of California, Davis, CA 95616, USA
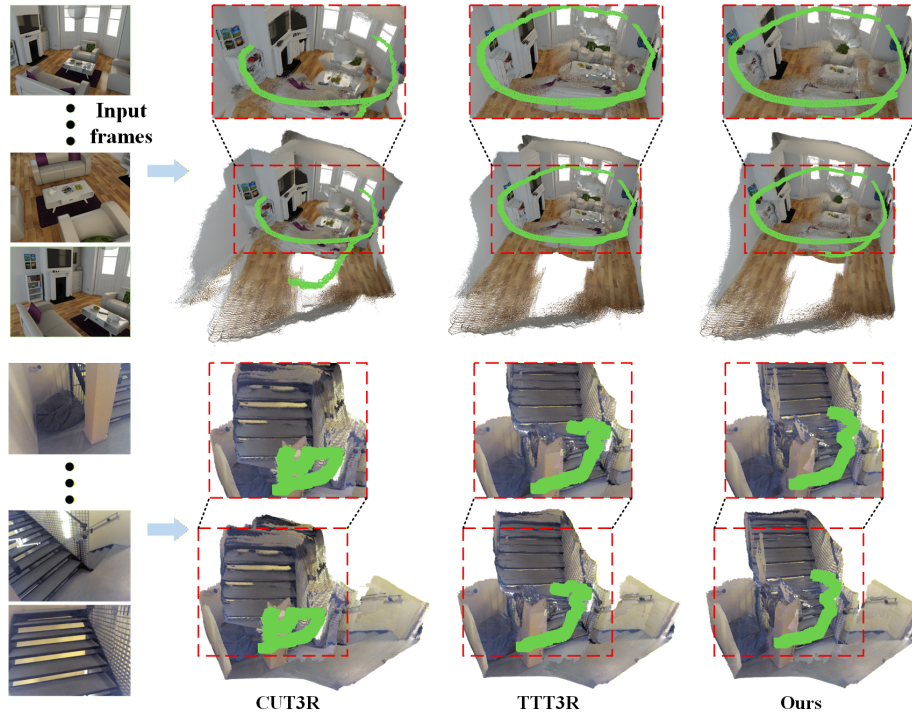{zhjzheng, xhxiang, jiwzhang}@ucdavis.edu

Fig. 1: Catastrophic forgetting in streaming 3D reconstruction. Given a sequence of input frames, CUT3R [49] with uniform updates suffers from severe pose drift and geometric distortions over long sequences (**left**). TTT3R [9] improves robustness but still exhibits artifacts (**middle**). Our method alleviates these issues through temporal-spatial adaptive updates to achieve coherent 3D reconstruction with accurate camera poses (**right**).

Abstract. Streaming recurrent models enable efficient 3D reconstruction by maintaining persistent state representations. However, they suffer

from catastrophic memory forgetting over long sequences due to balancing historical information with new observations. Recent methods alleviate this by deriving adaptive signals from attention perspective, but they operate on single dimensions without considering temporal and spatial consistency. To this end, we propose a training-free framework termed **TTSA3R** that leverages both temporal state evolution and spatial observation quality for adaptive state updates in 3D reconstruction. In particular, we devise a Temporal Adaptive Update Module that regulates update magnitude by analyzing temporal state evolution patterns. Then, a Spatial Contextual Update Module is introduced to localize spatial regions that require updates through observation-state alignment and scene dynamics. These complementary signals are finally fused to determine the state updating strategies. Extensive experiments demonstrate the effectiveness of TTSA3R in diverse 3D tasks. Moreover, our method exhibits only 15% error increase compared to over 200% degradation in baseline models on extended sequences, significantly improving long-term reconstruction stability. Our codes will be available soon.

Keywords: Streaming 3D Reconstruction · Training-free Adaptation · Temporal-Spatial Updates

1 Introduction

With the increasing demand for real-time 3D perception, understanding 3D scene structure from videos or images has become essential for applications including robotic manipulation and augmented reality, where spatial awareness enables safe interaction with the physical world. Traditional Structure-from-Motion (SfM) [30,38,44] and Multi-View Stereo (MVS) [7,21,22] pipelines obtain high-precision 3D reconstruction through iterative optimization but are limited by complex workflows and high computational cost. Recent transformer-based methods like DUSt3R [50] and VGGT [48] have demonstrated strong performance by joint reasoning across all frames with dense global attention [45], producing impressive reconstruction results on standard benchmarks. Nevertheless, the quadratic complexity of dense attention presents a fundamental limitation, as memory requirements scale quadratically with the number of frames, making these approaches impractical for the scenarios with long frame sequence inputs.

Streaming methods [11,12,29,54,57] have emerged as an alternative by processing frames incrementally to update the learned states without revisiting previous observations, enabling online reconstruction with reduced computational overhead. Existing approaches include spatial memory-based methods that anchor observations at 3D positions (Spann3R [47], Point3R [54]) and causal transformer architectures with key-value caching (STREAM3R [26], StreamVGGT [62]), which achieve efficient processing but suffer from unbounded memory growth as sequences extend. Alternatively, the recurrent model CUT3R [49] maintains compact persistent states with constant memory footprint and exhibits competitive accuracy.

However, extended sequences reveal limited length generalization due to catastrophic forgetting [9,10,28]. The uniform state update strategy [49] fails to prevent low-quality observations from overwriting historical information, which leads to accumulated errors and severe geometric distortions, as illustrated in Figure 1. In addition, spatial correspondence between states and observations is equally critical for determining update quality. To be specific, spatial interaction depends on both cross-attention alignment and feature consistency across frames. High cross-attention to regions with changing features indicates active geometric refinement, whereas cross-attention to regions with stable features suggests converged representations. Without jointly modeling these complementary signals, spatially irrelevant updates will corrupt stable geometry and necessary refinements may be missed. Recent training-free methods [9, 39] alleviate this issue through attention-based adaptive update mechanisms. However, these approaches only rely on single attention signals to guide state updates, which limits fine-grained state update control.

In this work, we present a training-free framework TTSA3R that mitigates the aforementioned issue through explicit temporal-spatial adaptive updates. We observe that state degradation stems from indiscriminate updates that fail to distinguish between stable geometry requiring preservation and outdated regions needing refinement. Therefore, effective updates should consider the analyses of both temporal and spatial signals. Specifically, temporal state evolution reveals the magnitude of change; spatial correspondence distinguishes whether high attention indicates active refinement with feature change or stable geometry with feature consistency. To this end, our approach introduces dedicated modules to analyze these complementary dimensions, thereby enabling fine-grained updates that preserve valuable information while integrating necessary observations.

To summarize, our main contributions are listed below:

• We propose a novel framework TTSA3R to alleviate long-term catastrophic forgetting for online streaming 3D reconstruction.

• We design a Temporal Adaptive Update Module (TAUM) based on state evolution analysis to track temporal state changes, which enables preservation of stable information and adapts to dynamic change.

• We introduce a Spatial Context Update Module (SCUM) combining cross-attention alignment and feature consistency to identify update-worthy regions, preventing erroneous updates when prior observations lack spatial coverage.

• Extensive experiments on video depth estimation, camera pose estimation, 3D reconstruction and diverse benchmarks demonstrate that our method achieves superior performance compared to state-of-the-art methods with real-time efficiency.

2   Related Work

Classical and Neural Rendering 3D Reconstruction. Traditional 3D reconstruction methods employ geometric optimization to recover spatial layout.

Structure-from-Motion [1,13,31,34,36,37,41,52] reconstruct scenes by establishing feature correspondences and refining camera parameters and 3D points. In contrast, Simultaneous Localization and Mapping (SLAM) [4, 15, 16, 18, 23, 33] performs joint localization and mapping in real-time. More recently, neural rendering methods including NeRF [6, 20, 32, 53] and 3DGS [5, 24, 43, 55, 58, 60] achieve photorealistic synthesis through per-scene optimization. However, they cannot generalize to novel scenes without retraining. This limitation motivates the development of generalizable learning-based reconstruction methods.

Feed-Forward 3D Reconstruction. Recent works develop feed-forward networks [46, 48, 50] for generalizable 3D reconstruction. Pairwise methods such as DUSt3R [50] directly regress pointmaps from image pairs using Vision Transformers, which eliminates the need for explicit feature matching. Building on this, MASt3R [27] extends [50] with pixel-level correspondences, while Fast3R [56] achieves real-time performance through architectural optimizations. For multi-view reconstruction, VGGT [48] processes all input frames jointly through global self-attention to model long-range dependencies across the sequence. FastVGGT [40] further reduces computational cost through a token merging strategy. Despite impressive performance, these feed-forward methods suffer from significant scalability issues. Global attention grows quadratically with the number of frames and processing all frames at once requires memory that increases linearly with sequence length. Consequently, these methods struggle with long input sequences. Therefore, streaming pipelines have emerged to enable continuous reconstruction and maintain fixed memory usage.

Streaming Online 3D Reconstruction. Current streaming methods provide a real-time and memory-efficient scheme for 3D reconstruction. Spann3R [47] maintains an external spatial memory that stores previous 3D predictions. CUT3R [49] introduces a recurrent transformer with persistent state tokens that accumulate information from sequential observations to achieve constant memory usage. Point3R [54] proposes explicit spatial pointer memory where each pointer is assigned a 3D position and aggregates nearby scene information. STREAM3R [26] reformulates reconstruction as a decoder-only transformer problem using causal attention. WinT3R [29] proposes a sliding window mechanism combined with a compact camera token pool, which enables direct interaction between adjacent frames. Nevertheless, these methods employ uniform update strategies that apply identical weights to all state tokens, causing accumulated errors and information forgetting during long-sequence reconstruction. To avoid costly training budget, recent researches shift to training-free approaches with the aim of utilizing adaptive signals during inference to alleviate this problem. TTT3R [9] derives adaptive learning rates from alignment confidence between new observations and history information. MUT3R [39] aggregates multi-layer self-attention to extract motion cues and suppresses dynamic regions through attention gating. However, the reliance on single-dimensional signals leads to suboptimal performance. Therefore, we propose to integrate temporal dynamics and spatial context, implementing decoupled adaptive control to balance long-term memory and noise suppression.

3   Method

Our framework TTSA3R maintains a fixed-size persistent state that encodes scene geometry and produces per-frame 3D reconstructions. As illustrated in Figure 2, it consists of two main components: Temporal Adaptive Update Module and Spatial Context Update Module. These two modules provide complementary signals that are integrated for fine-grained state updates.
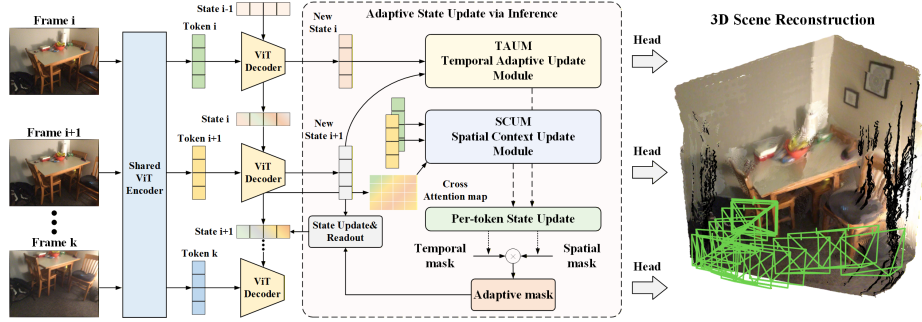

Fig. 2: Overview of our framework. Our method performs streaming 3D reconstruction from sequential frames through adaptively updating persistent state. A shared ViT encoder extracts visual tokens from input frames, which interact with the persistent state via ViT decoders to generate candidate states. Meanwhile, TAUM evaluates temporal state evolution across frames and SCUM measures spatial interaction between states and observations. Both modules produce complementary temporal and spatial masks, which are combined to update the persistent state at per-token granularity. Task-specific heads are utilized to predict depth maps, camera poses and pointmaps.

3.1   Preliminaries: CUT3R Inference

We firstly review the inference mechanism of CUT3R [49], which will be redesigned into an adaptive framework with the novel temporal and spatial update modules in this paper. The existing CUT3R model adopts a recurrent architecture that has a compact global persistent state for streaming 3D reconstruction. Given an input image sequence $\{I_1, ..., I_T\}$, each frame I_t is first encoded by models like ViT [17] into image tokens:

$$F_t = \text{Encoder}(I_t), \quad F_t \in \mathbb{R}^{K \times C} \tag{1}$$

where K denotes the number of patches and C is the feature dimension.

Based on encoding results, a shared-weight ViT decoder [50, 51] is used to process the current image tokens F_t together with the previous global state $S_{t-1} \in \mathbb{R}^{N \times C}$ and N is the number of state tokens. The decoder outputs new state tokens $\tilde{S}_t$ and multi-layer features D_t:

$$\tilde{S}_t, D_t = \text{Decoder}(F_t, S_{t-1}) \tag{2}$$

where $D_t = \left(D_t^{(0)}, ..., D_t^{(L)} \right)$ contains features from different decoder layers and L is the total decoder depth. These multi-layer features will be fed into a prediction head to obtain geometric outputs:

$$X_t, T_t, \text{conf}_t = \text{Head}(D_t) \tag{3}$$

where X_t denotes the predicted pointmap, T_t is the camera pose and conf_t represents per-pixel confidence. The global persistent state is subsequently updated through masked interpolation:

$$S_t = \tilde{S}_t \odot M + S_{t-1} \odot (1 - M) \tag{4}$$

where $M \in \{0, 1\}^{N \times 1}$ is a binary mask and $\odot$ denotes element-wise multiplication. In CUT3R, the mask is uniformly set to all ones, which directly replaces the previous state with new state tokens. Consequently, the model fully adapts to every new frame and constantly overwrites the global state. As sequences become longer, this uniform mechanism leads to catastrophic forgetting where historical information is progressively lost. Such information loss will cause geometric drift and degraded 3D reconstruction quality over extended sequences.

3.2 Temporal Adaptive Update Module

To mitigate the catastrophic forgetting problem [9,10,28], recent methods [9,39] capture adaptive updates from attention mechanisms. However, they mainly rely on intra-frame interactions within a single timestep, which lacks the ability to track inter-frame temporal changes. To this end, we propose the Temporal Adaptive Update Module (TAUM) to explicitly model how state representations vary over time and derive per-token update weights from temporal dynamics.

The core principle of TAUM is to differentiate update strategies by measuring the temporal stability from state change magnitudes across consecutive frames, which selectively preserves stable information and adapts to changing observations. Specifically, tokens that exhibit minimal variation across frames have likely converged to reliable geometric representations and benefit from preserving historical information to maintain long-term consistency. In contrast, tokens with significant variation indicate either time-varying scenes or unreliable estimates, both of which require aggressive updates to incorporate new observations.

In this paper, we formalize this principle through a per-token temporal adaptive mask as follows. To be specific, we measure the state evolution magnitude for each token and normalize the magnitude by the global average as:

$$\Delta_t = \text{Norm}(\tilde{S}_t - \tilde{S}_{t-1})$$
$$\hat{\Delta}_t = \Delta_t \left/ \left(\frac{1}{N} \sum_{i=1}^{N} \Delta_t^{(i)} \right) \right. \tag{5}$$

where $\text{Norm}(\cdot)$ computes the per-token L_2-norm across feature dimensions. This normalization is essential because it makes the change relative to the current

scene. Without normalization, the same absolute change value would have inconsistent semantic meanings across scenes with varying motion or geometric complexity. Then, we apply sigmoid gating to obtain the temporal mask as:

$$M_{\text{temp}} = \sigma(\hat{\Delta}_t - \tau) \tag{6}$$

where τ is a threshold parameter. Sigmoid-based gating provides smooth and differentiable control over update intensities. Tokens with normalized changes above τ incorporate new information, while tokens below τ retain their historical representations. Through this token-level adaptive mechanism, our design effectively alleviates the forgetting issue while maintaining the model's ability to capture dynamic scene changes.

3.3 Spatial Context Update Module

While TAUM mitigates temporal forgetting, it relies purely on temporal state tracking and neglects the spatial correspondence between states and observations. For instance, a token may change minimally across frames because prior views lacked coverage, yet current views provide new spatial information. Therefore, we propose the Spatial Context Update Module (SCUM) to provide complementary spatial awareness, as illustrated in Figure 3.

Specifically, our key insight is that spatial interaction reveals update necessity through two complementary signals. Cross-attention captures alignment confidence [9] between state tokens and image features. Additionally, feature divergence across consecutive frames distinguishes scene changes. Thus, high alignment confidence to regions undergoing substantial scene changes indicates active geometric refinement that requires updates. Otherwise, states will preserve their current representations.
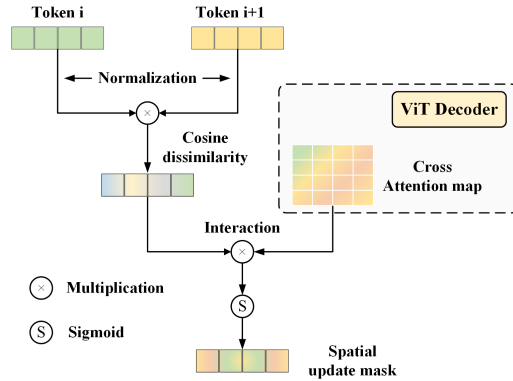

Fig. 3: Illustration of Spatial Context Update Module. Spatial update masks are generated by combining cosine dissimilarity and cross-attention signals through multiplication and sigmoid activation.

To achieve this, feature divergence is measured via cosine dissimilarity between consecutive frames as:

$$D_t = 1 - \text{CosSim}(F_t, F_{t-1}) \tag{7}$$

where F_t denotes image features at timestep t. Cross-attention maps from the decoder layers are aggregated to quantify how strongly each state token engages with image observations as:

$$A_t = \frac{1}{L} \sum_{l=1}^{L} |\text{CrossAttn}^{(l)}(S_{t-1}, F_t)| \tag{8}$$

where L is the number of decoder layers. The spatial interaction is computed as the element-wise product of attention and dissimilarity, followed by max pooling across image tokens and sigmoid gating to derive the spatial mask as:

$$M_{\text{spat}} = \sigma(max_{\text{spat}}(A_t \odot D_t)) \tag{9}$$

The element-wise product $\odot$ ensures high activation only when both attention and divergence are substantial. Spatial max pooling max_{spat} exploits the observation that each state token typically corresponds to specific image regions. Sigmoid activation normalizes the mask to $[0, 1]$. SCUM thereby updates tokens that engage with evolving scene geometry while preserving those that correspond to stable regions. This provides spatial awareness that complements TAUM's temporal perspective.

Finally, in order to integrate these complementary perspectives, we combine TAUM and SCUM to obtain the adaptive mask as:

$$M_{\text{final}} = M_{\text{temp}} \odot M_{\text{spat}} \tag{10}$$

This fusion ensures updates only when both temporal dynamics and spatial correspondence are met. Then, the global state update is illustrated as:

$$S_t = \tilde{S}_t \odot M_{\text{final}} + S_{t-1} \odot (1 - M_{\text{final}}) \tag{11}$$

By extracting complementary temporal and spatial signals from internal decoder representations, TTSA3R alleviates catastrophic forgetting in streaming 3D reconstruction. This enables the model to maintain long-term consistency across extended sequences while adapting to new observations.

4 Experiments

Implementation Details. We conduct experiments on three tasks including video depth estimation, camera pose estimation, and 3D reconstruction. Following the common practice [9,49,62], we assess video depth on Sintel [3], Bonn [35], and KITTI [19] datasets, where we report absolute relative error (Abs Rel) and

Table 1: Video Depth Estimation on standard short sequences. We evaluate scale-invariant and metric depth accuracy on Sintel [3], Bonn [35], and KITTI [19] datasets. Methods that require global alignment are denoted as "GA". "Optim", "Stream", and "FA" refer to optimization-based, streaming, and full-attention methods, respectively. The best and second best results are marked in bold and underline.

Alignment	Method	Type	Sintel		Bonn		KITTI	
			Abs Rel $\downarrow$	$\delta < 1.25 \uparrow$	Abs Rel $\downarrow$	$\delta < 1.25 \uparrow$	Abs Rel $\downarrow$	$\delta < 1.25 \uparrow$
Per-sequence scale	DUSt3R-GA [50]	Optim	0.656	45.2	0.155	83.3	0.144	81.3
	MASt3R-GA [27]	Optim	0.641	43.9	0.252	70.1	0.183	74.5
	MonST3R-GA [59]	Optim	0.378	55.8	0.067	96.3	0.168	74.4
	Easi3R [8]	FA	0.377	55.9	0.059	97.0	0.102	91.2
	VGGT [48]	FA	**0.287**	**66.1**	**0.055**	97.1	**0.070**	**96.5**
	Spann3R [47]	Stream	0.622	42.6	0.144	81.3	0.198	73.7
	Point3R [54]	Stream	0.452	48.9	0.060	96.0	0.136	84.2
	CUT3R [49]	Stream	0.421	47.9	0.078	93.7	0.118	88.1
	TTT3R [9]	Stream	0.405	48.9	0.069	95.4	0.114	90.4
	STREAM3R$^\alpha$ [26]	Stream	0.478	51.1	0.075	94.1	0.116	89.6
	StreamVGGT [62]	Stream	0.323	65.7	0.059	**97.2**	0.173	72.1
	MUT3R [39]	Stream	0.451	48.6	0.070	96.2	0.116	88.3
	Ours	Stream	0.401	50.0	0.064	96.5	**0.110**	**91.2**
Metric scale	MASt3R-GA [27]	Optim	1.022	14.3	0.272	70.6	0.467	15.2
	CUT3R [49]	Stream	1.029	23.8	0.103	88.5	0.122	85.5
	Point3R [54]	Stream	**0.777**	17.1	0.137	94.7	0.191	73.8
	TTT3R [9]	Stream	0.977	24.5	0.090	94.2	**0.110**	**89.1**
	STREAM3R$^\alpha$ [26]	Stream	1.041	21.0	0.084	94.4	0.234	57.6
	MUT3R [39]	Stream	0.820	**25.2**	0.086	96.0	0.125	85.8
	Ours	Stream	0.960	24.6	**0.079**	**96.6**	0.111	88.9

the percentage of pixels with relative error below 1.25 ($\delta < 1.25$). We then evaluate camera pose estimation on Sintel, TUM-dynamics [42], and ScanNet [14] datasets, measuring Absolute Translation Error (ATE), Relative Translation Error ($\text{RPE}_{\text{trans}}$), and Relative Rotation Error (RPE_{rot}) after Sim(3) alignment with ground truth. For 3D reconstruction, we use NRGBD [2] dataset and report accuracy (Acc) as well as normal consistency (NC). We compare against methods grouped by different processing paradigms. Optimization-based methods like DUSt3R-GA [50], MASt3R-GA [27], and MonST3R-GA [59] perform global refinement over images. Full-attention methods such as Easi3R [8] and VGGT [48] process all frames jointly via bidirectional attention. Streaming methods including Spann3R [47], Point3R [54], CUT3R [49], TTT3R [9], STREAM3R [26], StreamVGGT [62], and MUT3R [39] maintain frame-by-frame inference. All experiments are performed on a single NVIDIA A6000 GPU.

4.1 Video Depth Estimation

We evaluate video depth on both short and long sequences. Table 1 shows the results on standard benchmarks under two evaluation protocols, which are per-sequence scale and metric scale directly comparing absolute depth values. Under per-sequence scale, our method TTSA3R achieves the best performance among streaming methods on KITTI [19] dataset while maintaining competitive on the other two datasets. Moreover, TTSA3R demonstrates superior performance on
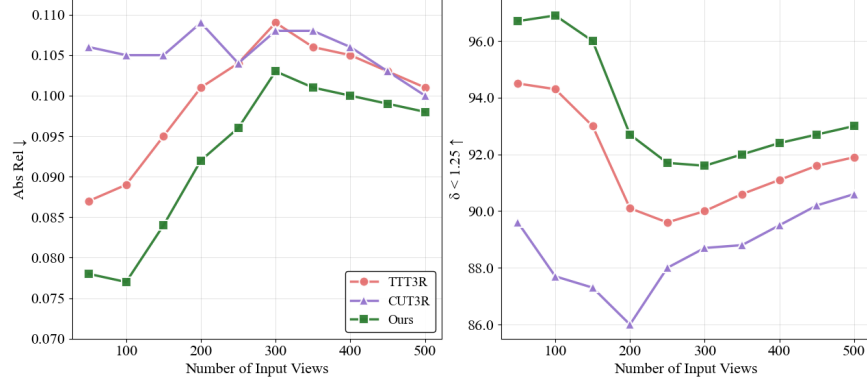
Fig. 4: Video depth estimation (long sequences) using metric depth accuracy on Bonn [35] dataset.

Bonn [35] dataset and approaches the performance of full-attention pipelines based on metric scale, narrowing the gap between online and offline methods.

Figure 4 illustrates how video depth evolves as input sequence length increases from 50 to 500 frames. It can be seen that CUT3R [49] exhibits rapid performance degradation beyond 200 frames due to catastrophic forgetting. TTT3R [9] presents improved stability through confidence guided adaptation but still suffers from gradual drift in longer sequences. On the contrary, TTSA3R obtains more robust performance throughout the varying sequences with minor degradation. This illustrates that our temporal-spatial fusion effectively reduces long-term error accumulation and preserves geometric fidelity.

Table 2: Camera Pose Estimation on standard short sequences. We evaluate three metrics on Sintel [3], TUM-dynamics [42], and ScanNet [14] datasets .

Method	Type	Sintel			TUM-dynamics			ScanNet		
		ATE ↓	RPE trans ↓	RPE rot ↓	ATE ↓	RPE trans ↓	RPE rot ↓	ATE ↓	RPE trans ↓	RPE rot ↓
Robust-CVD [25]	Optim	0.360	0.154	3.443	0.153	0.026	3.528	0.227	0.064	7.374
CasualSAM [61]	Optim	0.141	**0.035**	0.615	0.071	**0.010**	1.712	0.158	0.034	1.618
DUSt3R-GA [50]	Optim	0.417	0.250	5.796	0.083	0.017	3.567	0.081	0.028	0.784
MASt3R-GA [27]	Optim	0.185	0.060	1.496	0.038	0.012	0.448	0.078	0.020	0.475
MonST3R-GA [59]	Optim	0.111	0.044	0.869	0.098	0.019	0.935	0.077	0.018	0.529
Easi3R [8]	FA	0.110	0.042	0.758	0.105	0.022	1.064	0.061	0.017	0.525
VGGT [48]	FA	0.172	0.062	**0.471**	**0.012**	**0.010**	**0.310**	**0.035**	**0.015**	**0.377**
Spann3R [47]	Stream	0.329	0.110	4.471	0.056	0.021	0.591	0.096	0.023	0.661
CUT3R [49]	Stream	0.213	0.066	**0.621**	0.046	0.015	0.473	0.099	0.022	0.600
Point3R [54]	Stream	0.351	0.128	1.822	0.075	0.029	0.642	0.106	0.035	1.946
TTT3R [9]	Stream	**0.210**	0.090	0.722	0.028	0.013	0.380	0.064	0.021	0.637
MUT3R [39]	Stream	0.228	**0.062**	0.751	0.042	0.015	0.445	-	-	-
Ours	Stream	**0.210**	0.085	0.765	**0.026**	**0.012**	0.372	**0.057**	**0.020**	**0.588**

4.2   Camera Pose Estimation

To validate the effectiveness of our method, we next conduct experiments on camera pose estimation. Table 2 presents the quantitative results across Sintel [3], TUM-dynamics [42], and ScanNet [14] datasets. It is shown that TTSA3R achieves the lowest ATE among streaming methods on TUM-dynamics and Scannet datasets. It outperforms optimization-based pipelines like DUSt3R-GA [50] with global alignment and matches full-attention baselines such as Easi3R [8]. Besides, we also evaluate pose tracking on sequences up to 800 frames for long-term stability assessment, as illustrated in Figure 5. Across both datasets, it can be seen that our method TTSA3R maintains significantly lower pose error and surpasses the other two methods.
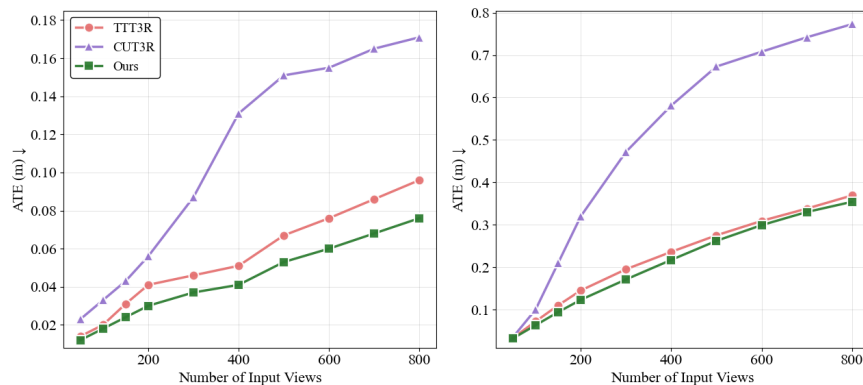

Fig. 5: Camera pose estimation (long sequences) on TUM-dynamics [42] (left) and ScanNet [14] (right) datasets.

4.3   3D Reconstruction

We further evaluate 3D reconstruction on NRGBD [2] dataset across different sequences. The quantitative results are shown in Figure 6. Compared to CUT3R [49] and TTT3R [9], our method shows better performance on all sequence lengths, which exhibits effective resistance to memory forgetting problem.

Moreover, qualitative visualizations of scene reconstruction are provided in Figure 7. It is clear that CUT3R produces severely distorted geometry and less accurate camera trajectory. Although TTT3R mitigates these issues and has reformative quality, the residual artifacts and surface inconsistencies remain visible. Instead, our method generates more coherent reconstruction results with accurate scene structure. This shows that our proposed framework with selective state update strategy successfully achieves the balance between preserving historical information and incorporating new observations.
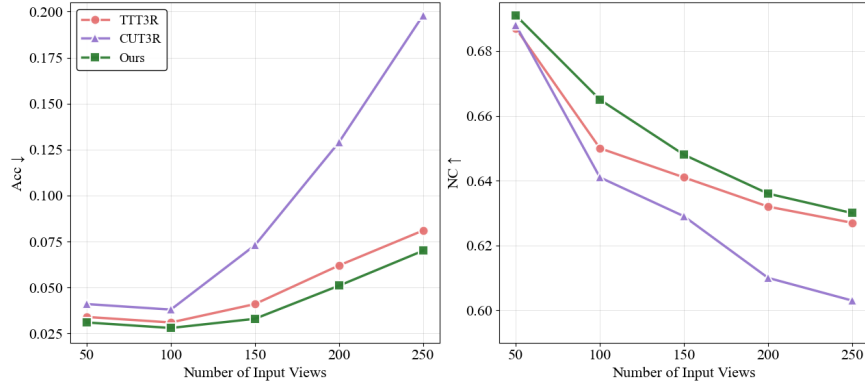
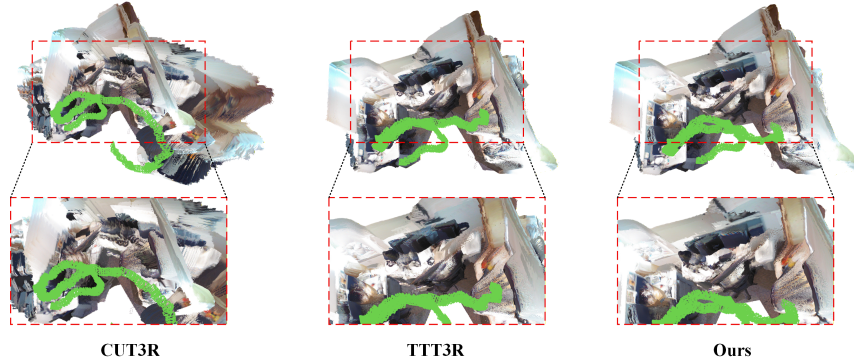**Fig. 6: 3D reconstruction** (long sequences) on NRGBD [2] dataset.

Fig. 7: Qualitative comparison of 3D reconstruction. Our method can produce more complete and accurate reconstructions. Please refer to the Supplementary materials for more visualization comparisons.

4.4   Ablation Studies and Analysis

Effect of Each Component. To assess the contribution of each module, we conduct ablation studies on Bonn [35] and TUM-dynamics [42] datasets using CUT3R [49] as the baseline. As shown in Table 3, when we only add TAUM to the baseline, it achieves 0.066 Abs Rel on video depth and 0.028 ATE on camera pose. This indicates that TAUM effectively mitigates error accumulation by adaptively controlling update magnitude based on temporal state evolution, which is particularly beneficial for maintaining trajectory consistency in pose estimation. Adding SCUM alone obtains 0.074 Abs Rel and 0.040 ATE, respectively. This shows that SCUM identifies spatial changing regions for updates based on observation-state alignment, preventing uniform updates across areas. When both modules are integrated into the framework, TTSA3R achieves the

Table 3: Ablation studies of each component. We evaluate video depth estimation on Bonn [35] dataset and camera pose estimation on TUM-dynamics [42] dataset.

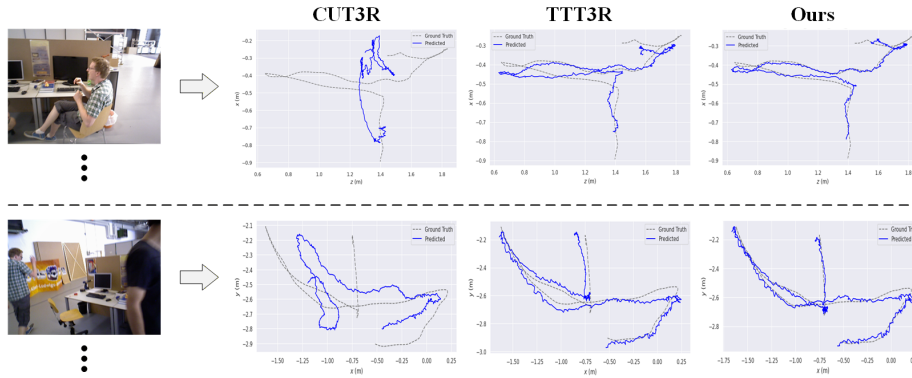| Method			Bonn		TUM-dynamics	
			Abs Rel $\downarrow$	$\delta < 1.25 \uparrow$	ATE $\downarrow$	RPE rot $\downarrow$
Baseline			0.078	93.7	0.046	0.473
TAUM	✓		0.066	95.9	0.028	0.375
SCUM		✓	0.074	94.1	0.040	0.415
Ours	✓	✓	**0.064**	**96.5**	**0.026**	**0.372**

Fig. 8: Qualitative comparison of predicted camera trajectories on TUM-dynamics [42] dataset. The trajectories are visualized along the two axes with maximum variance. Gray dashed lines show ground truth and blue lines show predictions.

best performance with 0.064 Abs Rel and 0.026 ATE. This verifies that temporal-spatial adaptive updates effectively alleviate memory forgetting by selectively refining state representation.

Camera Trajectory Analysis. We visualize predicted camera trajectories on TUM-dynamics [42] dataset to analyse pose estimation. Figure 8 presents two representative sequences from indoor scenes with moving persons. It can be seen that the trajectories of CUT3R [49] reveal progressive drift accumulation during continuous motion and abrupt deviations during rapid viewpoint changes. Though recent approaches like TTT3R [9] reduce drift magnitude, noticeable deviations from the reference path remain. These observations reflect how existing recurrent methods lack effective adaptive mechanisms that respond to varying observations and temporal dynamics. Our predicted trajectories closely align with the reference path throughout the sequence. The consistent accuracy stems from jointly evaluating temporal state evolution and spatial observation quality during updates, which prevents error propagation in both gradual drift and abrupt viewpoint changes, thus enabling more robust trajectory estimation.
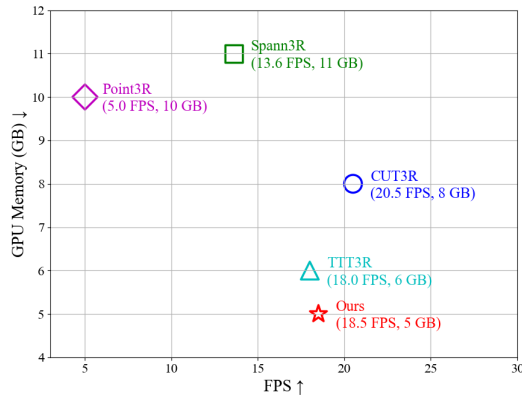
Fig. 9: Comparison of inference efficiency. We compare GPU memory used and FPS of different methods using 512×144 image resolution on KITTI [19] dataset.

Inference Efficiency Analysis. We further evaluate computational efficiency by measuring inference speed and GPU memory consumption on video depth estimation. As illustrated in Figure 9, spatial memory-based methods Spann3R [47] and Point3R [54] suffer from substantial memory overhead. Conversely, CUT3R [49] preserves constant memory but its performance degrades on extended sequences. Similarly, TTT3R [9] improves memory efficiency by achieving 6 GB consumption. Notably, TTSA3R achieves the lowest memory footprint at 5 GB with 18.5 FPS inference speed. These results demonstrate that our method achieves a competitive efficiency-memory trade-off among existing streaming methods.

5   Conclusions

In this work, we present a training-free 3D reconstruction framework TTSA3R that mitigates catastrophic memory forgetting of recurrent models for streaming reconstruction through an adaptive temporal-spatial mechanism. Specifically, the key contribution is a dual-module design that models temporal state dynamics and spatial correspondence, enabling complementary selective updates based on cross-frame evolution and observation quality. Consequently, this approach enables fine-grained control over memory persistence with real-time inference efficiency. Extensive experiments demonstrate that our method achieves competitive or superior performance compared to state-of-the-art pipelines across different benchmarks and tasks.

Limitations. Our method is optimized for extended streaming scenarios with adequate visual overlap. Performance degrades under severe occlusions or sparse observations where correspondence signals become unreliable. Additionally, as a training-free design, the adaptive mechanism is inherently limited by the representational capacity of the base recurrent architecture.

References

1. Agarwal, S., Furukawa, Y., Snavely, N., Simon, I., Curless, B., Seitz, S.M., Szeliski, R.: Building rome in a day. Communications of the ACM **54**(10), 105–112 (2011)
2. Azinović, D., Martin-Brualla, R., Goldman, D.B., Nießner, M., Thies, J.: Neural rgb-d surface reconstruction. In: Proceedings of the IEEE/CVF Conference on Computer Vision and Pattern Recognition. pp. 6290–6301 (2022)
3. Butler, D.J., Wulff, J., Stanley, G.B., Black, M.J.: A naturalistic open source movie for optical flow evaluation. In: European conference on computer vision. pp. 611–625. Springer (2012)
4. Cadena, C., Carlone, L., Carrillo, H., Latif, Y., Scaramuzza, D., Neira, J., Reid, I., Leonard, J.J.: Past, present, and future of simultaneous localization and mapping: Toward the robust-perception age. IEEE Transactions on robotics **32**(6), 1309–1332 (2017)
5. Charatan, D., Li, S.L., Tagliasacchi, A., Sitzmann, V.: pixelsplat: 3d gaussian splats from image pairs for scalable generalizable 3d reconstruction. In: Proceedings of the IEEE/CVF conference on computer vision and pattern recognition. pp. 19457–19467 (2024)
6. Chen, H., Gu, J., Chen, A., Tian, W., Tu, Z., Liu, L., Su, H.: Single-stage diffusion nerf: A unified approach to 3d generation and reconstruction. In: Proceedings of the IEEE/CVF international conference on computer vision. pp. 2416–2425 (2023)
7. Chen, R., Han, S., Xu, J., Su, H.: Point-based multi-view stereo network. In: Proceedings of the IEEE/CVF international conference on computer vision. pp. 1538–1547 (2019)
8. Chen, X., Chen, Y., Xiu, Y., Geiger, A., Chen, A.: Easi3r: Estimating disentangled motion from dust3r without training. arXiv preprint arXiv:2503.24391 (2025)
9. Chen, X., Chen, Y., Xiu, Y., Geiger, A., Chen, A.: Ttt3r: 3d reconstruction as test-time training. arXiv preprint arXiv:2509.26645 (2025)
10. Chen, X., Xia, T., Xu, S., Yang, J., Chai, J., Cheng, Z.: Sab3r: Semantic-augmented backbone in 3d reconstruction. arXiv preprint arXiv:2506.02112 (2025)
11. Chen, Y., Chen, X., Xue, Y., Chen, A., Xiu, Y., Pons-Moll, G.: Human3r: Everyone everywhere all at once. arXiv preprint arXiv:2510.06219 (2025)
12. Chen, Z., Qin, M., Yuan, T., Liu, Z., Zhao, H.: Long3r: Long sequence streaming 3d reconstruction. In: Proceedings of the IEEE/CVF International Conference on Computer Vision. pp. 5273–5284 (2025)
13. Cui, H., Gao, X., Shen, S., Hu, Z.: Hsfm: Hybrid structure-from-motion. In: Proceedings of the IEEE conference on computer vision and pattern recognition. pp. 1212–1221 (2017)
14. Dai, A., Chang, A.X., Savva, M., Halber, M., Funkhouser, T., Nießner, M.: Scannet: Richly-annotated 3d reconstructions of indoor scenes. In: Proceedings of the IEEE conference on computer vision and pattern recognition. pp. 5828–5839 (2017)
15. Davison: Real-time simultaneous localisation and mapping with a single camera. In: Proceedings Ninth IEEE International Conference on Computer Vision. pp. 1403–1410. IEEE (2003)
16. Davison, A.J., Reid, I.D., Molton, N.D., Stasse, O.: Monoslam: Real-time single camera slam. IEEE transactions on pattern analysis and machine intelligence **29**(6), 1052–1067 (2007)
17. Dosovitskiy, A.: An image is worth 16x16 words: Transformers for image recognition at scale. arXiv preprint arXiv:2010.11929 (2020)

18. Durrant-Whyte, H., Bailey, T.: Simultaneous localization and mapping: part i. IEEE robotics & automation magazine **13**(2), 99–110 (2006)
19. Geiger, A., Lenz, P., Stiller, C., Urtasun, R.: Vision meets robotics: The kitti dataset. The international journal of robotics research **32**(11), 1231–1237 (2013)
20. Guo, Y., Kumar, A., Zhao, C., Wang, R., Huang, X., Ren, L.: Sup-nerf: A streamlined unification of pose estimation and nerf for monocular 3d object reconstruction. In: European Conference on Computer Vision. pp. 37–53. Springer (2024)
21. Habbecke, M., Kobbelt, L.: A surface-growing approach to multi-view stereo reconstruction. In: 2007 IEEE Conference on Computer Vision and Pattern Recognition. pp. 1–8. IEEE (2007)
22. Hepp, B., Nießner, M., Hilliges, O.: Plan3d: Viewpoint and trajectory optimization for aerial multi-view stereo reconstruction. ACM Transactions on Graphics (TOG) **38**(1), 1–17 (2018)
23. Huang, H., Li, L., Cheng, H., Yeung, S.K.: Photo-slam: Real-time simultaneous localization and photorealistic mapping for monocular stereo and rgb-d cameras. In: Proceedings of the IEEE/CVF Conference on Computer Vision and Pattern Recognition. pp. 21584–21593 (2024)
24. Kerbl, B., Kopanas, G., Leimkühler, T., Drettakis, G.: 3d gaussian splatting for real-time radiance field rendering. ACM Transactions on Graphics **42**(4), 1–14 (2023)
25. Kopf, J., Rong, X., Huang, J.B.: Robust consistent video depth estimation. In: Proceedings of the IEEE/CVF Conference on Computer Vision and Pattern Recognition. pp. 1611–1621 (2021)
26. Lan, Y., Luo, Y., Hong, F., Zhou, S., Chen, H., Lyu, Z., Yang, S., Dai, B., Loy, C.C., Pan, X.: Stream3r: Scalable sequential 3d reconstruction with causal transformer. arXiv preprint arXiv:2508.10893 (2025)
27. Leroy, V., Cabon, Y., Revaud, J.: Grounding image matching in 3d with mast3r. In: European Conference on Computer Vision. pp. 71–91. Springer (2024)
28. Li, F., Hu, P., Song, Q., Huang, R.: Incremental 3d reconstruction through a hybrid explicit-and-implicit representation. In: 2024 IEEE International Conference on Robotics and Automation (ICRA). pp. 15121–15127. IEEE (2024)
29. Li, Z., Zhou, J., Wang, Y., Guo, H., Chang, W., Zhou, Y., Zhu, H., Chen, J., Shen, C., He, T.: Wint3r: Window-based streaming reconstruction with camera token pool. arXiv preprint arXiv:2509.05296 (2025)
30. Lindenberger, P., Sarlin, P.E., Larsson, V., Pollefeys, M.: Pixel-perfect structure-from-motion with featuremetric refinement. In: Proceedings of the IEEE/CVF international conference on computer vision. pp. 5987–5997 (2021)
31. Liu, S., Gao, Y., Zhang, T., Pautrat, R., Schönberger, J.L., Larsson, V., Pollefeys, M.: Robust incremental structure-from-motion with hybrid features. In: European Conference on Computer Vision. pp. 249–269. Springer (2024)
32. Mildenhall, B., Srinivasan, P.P., Tancik, M., Barron, J.T., Ramamoorthi, R., Ng, R.: Nerf: Representing scenes as neural radiance fields for view synthesis. Communications of the ACM **65**(1), 99–106 (2021)
33. Newcombe, R.A., Lovegrove, S.J., Davison, A.J.: Dtam: Dense tracking and mapping in real-time. In: 2011 international conference on computer vision. pp. 2320–2327. IEEE (2011)
34. Ni, K., Steedly, D., Dellaert, F.: Out-of-core bundle adjustment for large-scale 3d reconstruction. In: 2007 IEEE 11th International Conference on Computer Vision. pp. 1–8. IEEE (2007)

35. Palazzolo, E., Behley, J., Lottes, P., Giguere, P., Stachniss, C.: Refusion: 3d reconstruction in dynamic environments for rgb-d cameras exploiting residuals. In: 2019 IEEE/RSJ International Conference on Intelligent Robots and Systems (IROS). pp. 7855–7862. IEEE (2019)

36. Pinard, C., Chevalley, L., Manzanera, A., Filliat, D.: Learning structure-from-motion from motion. In: Proceedings of the European Conference on Computer Vision (ECCV) Workshops. pp. 0–0 (2018)

37. Schonberger, J.L., Frahm, J.M.: Structure-from-motion revisited. In: Proceedings of the IEEE conference on computer vision and pattern recognition. pp. 4104–4113 (2016)

38. Shah, R., Deshpande, A., Narayanan, P.: Multistage sfm: Revisiting incremental structure from motion. In: 2014 2nd International Conference on 3D Vision. vol. 1, pp. 417–424. IEEE (2014)

39. Shen, G., Deng, T., Qin, X., Wang, N., Wang, J., Wang, Y., Chen, Y., Wang, H., Wang, J.: Mut3r: Motion-aware updating transformer for dynamic 3d reconstruction. arXiv preprint arXiv:2512.03939 (2025)

40. Shen, Y., Zhang, Z., Qu, Y., Zheng, X., Ji, J., Zhang, S., Cao, L.: Fastvggt: Training-free acceleration of visual geometry transformer. arXiv preprint arXiv:2509.02560 (2025)

41. Snavely, N., Seitz, S.M., Szeliski, R.: Photo tourism: exploring photo collections in 3d. In: ACM siggraph 2006 papers, pp. 835–846 (2006)

42. Sturm, J., Engelhard, N., Endres, F., Burgard, W., Cremers, D.: A benchmark for the evaluation of rgb-d slam systems. In: 2012 IEEE/RSJ international conference on intelligent robots and systems. pp. 573–580. IEEE (2012)

43. Tang, J., Gao, Y., Yang, D., Yan, L., Yue, Y., Yang, Y.: Dronesplat: 3d gaussian splatting for robust 3d reconstruction from in-the-wild drone imagery. In: Proceedings of the Computer Vision and Pattern Recognition Conference. pp. 833–843 (2025)

44. Torresani, L., Hertzmann, A., Bregler, C.: Nonrigid structure-from-motion: Estimating shape and motion with hierarchical priors. IEEE transactions on pattern analysis and machine intelligence **30**(5), 878–892 (2008)

45. Vaswani, A., Shazeer, N., Parmar, N., Uszkoreit, J., Jones, L., Gomez, A.N., Kaiser, Ł., Polosukhin, I.: Attention is all you need. Advances in neural information processing systems **30** (2017)

46. Wang, C.S.B., Schmidt, C., Piekenbrinck, J., Leibe, B.: Faster vggt with block-sparse global attention. arXiv preprint arXiv:2509.07120 (2025)

47. Wang, H., Agapito, L.: 3d reconstruction with spatial memory. arXiv preprint arXiv:2408.16061 (2024)

48. Wang, J., Chen, M., Karaev, N., Vedaldi, A., Rupprecht, C., Novotny, D.: Vggt: Visual geometry grounded transformer. In: Proceedings of the Computer Vision and Pattern Recognition Conference. pp. 5294–5306 (2025)

49. Wang, Q., Zhang, Y., Holynski, A., Efros, A.A., Kanazawa, A.: Continuous 3d perception model with persistent state. In: Proceedings of the Computer Vision and Pattern Recognition Conference. pp. 10510–10522 (2025)

50. Wang, S., Leroy, V., Cabon, Y., Chidlovskii, B., Revaud, J.: Dust3r: Geometric 3d vision made easy. In: Proceedings of the IEEE/CVF Conference on Computer Vision and Pattern Recognition. pp. 20697–20709 (2024)

51. Weinzaepfel, P., Leroy, V., Lucas, T., Brégier, R., Cabon, Y., Arora, V., Antsfeld, L., Chidlovskii, B., Csurka, G., Revaud, J.: Croco: Self-supervised pre-training for 3d vision tasks by cross-view completion. Advances in Neural Information Processing Systems **35**, 3502–3516 (2022)

52. Wu, C.: Towards linear-time incremental structure from motion. In: 2013 International Conference on 3D Vision-3DV 2013. pp. 127–134. IEEE (2013)
53. Wu, R., Mildenhall, B., Henzler, P., Park, K., Gao, R., Watson, D., Srinivasan, P.P., Verbin, D., Barron, J.T., Poole, B., et al.: Reconfusion: 3d reconstruction with diffusion priors. In: Proceedings of the IEEE/CVF conference on computer vision and pattern recognition. pp. 21551–21561 (2024)
54. Wu, Y., Zheng, W., Zhou, J., Lu, J.: Point3r: Streaming 3d reconstruction with explicit spatial pointer memory. arXiv preprint arXiv:2507.02863 (2025)
55. Xiang, H., Li, X., Cheng, K., Lai, X., Zhang, W., Liao, Z., Zeng, L., Liu, X.: Gaussianroom: Improving 3d gaussian splatting with sdf guidance and monocular cues for indoor scene reconstruction. In: 2025 IEEE International Conference on Robotics and Automation (ICRA). pp. 2686–2693. IEEE (2025)
56. Yang, J., Sax, A., Liang, K.J., Henaff, M., Tang, H., Cao, A., Chai, J., Meier, F., Feiszli, M.: Fast3r: Towards 3d reconstruction of 1000+ images in one forward pass. In: Proceedings of the Computer Vision and Pattern Recognition Conference. pp. 21924–21935 (2025)
57. Yuan, Y., Shen, Q., Wang, S., Yang, X., Wang, X.: Test3r: Learning to reconstruct 3d at test time. In: The Thirty-ninth Annual Conference on Neural Information Processing Systems (2025)
58. Yuan, Z., Huang, H., Xiong, Z., Wang, D., Yang, G.: Robust and efficient 3d gaussian splatting for urban scene reconstruction. In: Proceedings of the IEEE/CVF International Conference on Computer Vision. pp. 26209–26219 (2025)
59. Zhang, J., Herrmann, C., Hur, J., Jampani, V., Darrell, T., Cole, F., Sun, D., Yang, M.H.: Monst3r: A simple approach for estimating geometry in the presence of motion. arXiv preprint arXiv:2410.03825 (2024)
60. Zhang, K., Bi, S., Tan, H., Xiangli, Y., Zhao, N., Sunkavalli, K., Xu, Z.: Gs-lrm: Large reconstruction model for 3d gaussian splatting. In: European Conference on Computer Vision. pp. 1–19. Springer (2024)
61. Zhang, Z., Cole, F., Li, Z., Rubinstein, M., Snavely, N., Freeman, W.T.: Structure and motion from casual videos. In: European Conference on Computer Vision. pp. 20–37. Springer (2022)
62. Zhuo, D., Zheng, W., Guo, J., Wu, Y., Zhou, J., Lu, J.: Streaming 4d visual geometry transformer. arXiv preprint arXiv:2507.11539 (2025)